crystals

MDPI

Article

Ultrasound-Assisted Synthesis and DFT Calculations of the Novel 1D Pb (II) Coordination Polymer with Thiosemicarbazone Derivative Ligand and Its Use for Preparation of PbO Clusters

Jaber Dadashi [1], Younes Hanifehpour [2,*], Babak Mirtamizdoust [1], Mehdi Abdolmaleki [2], Elham Mohammadi Jegarkandi [1], Mahboubeh Rezaei [1] and Sang Woo Joo [3,*]

[1] Department of Chemistry, Faculty of Science, University of Qom, Qom P.O. Box 37185-359, Iran; jaber_dadashi_95@yahoo.com (J.D.); babakm.tamizdoust@gmail.com (B.M.); mahboubeh.rezaei1998@gmail.com (E.M.J.); Mohammadi.elham2021@gmail.com (M.R.)
[2] Department of Chemistry, Sayyed Jamaleddin Asadabadi University, Asadabad 6541861841, Iran; m.abdolmaleki@sjau.ac.ir
[3] School of Mechanical Engineering, WCU Nano Research Center, Yeungnam University, Gyeongsan 712-749, Korea
* Correspondence: Hanifehpour@sjau.ac.ir (Y.H.); swjoo@yu.ac.kr (S.W.J.)

check for updates

Citation: Dadashi, J.; Hanifehpour, Y.; Mirtamizdoust, B.; Abdolmaleki, M.; Jegarkandi, E.M.; Rezaei, M.; Joo, S.W. Ultrasound-Assisted Synthesis and DFT Calculations of the Novel 1D Pb (II) Coordination Polymer with Thiosemicarbazone Derivative Ligand and Its Use for Preparation of PbO Clusters. *Crystals* **2021**, *11*, 682. https://doi.org/10.3390/cryst11060682

Academic Editor: Ana M. Garcia-Deibe

Received: 13 April 2021
Accepted: 11 June 2021
Published: 14 June 2021

Publisher's Note: MDPI stays neutral with regard to jurisdictional claims in published maps and institutional affiliations.

Copyright: © 2021 by the authors. Licensee MDPI, Basel, Switzerland. This article is an open access article distributed under the terms and conditions of the Creative Commons Attribution (CC BY) license (https://creativecommons.org/licenses/by/4.0/).

Abstract: In the present work, using a sonochemical method, a new lead (II) coordination 1D polymer, $[Pb(L)_2(CH_3COO)]_n$ (L = pyridine-4-carbaldehyde thiosemicarbazone) (**1**) was prepared. It was characterized structurally with different spectroscopic methods, such as SEM, IR spectroscopy, XRD, and elemental analysis. The coordination compound becomes a stair-step one-dimensional polymer in solid mode. The lead (II) ions have the coordination number of six ($PbNS_3O_2$) with two oxygen atoms from acetate anion and three sulfur atoms and one nitrogen atom from organic ligand. It contains a stereo-chemically active lone electron pair and the hemidirected coordination sphere. The high-intensity ultrasound is considered a flexible, environmentally friendly, and easy synthetic tool for the coordination compounds. PbO clusters was achieved with thermolyzing **1** at 180 °C with oleic acid (as a surfactant). Furthermore, the size and morphology of the created PbO clusters were assessed via SEM. The estimated gap of HOMO and LUMO is 3.275 eV based on DFT calculations.

Keywords: coordination compound; crystal structure; X-ray crystallography; ultrasonic irradiation; Pb(II) complex

1. Introduction:

Metal organic coordination polymers are researched commonly within inorganic chemistry [1]. Drug delivery [2], liquid and gas separation [3], sensor technology [4], heterogeneous catalysis [5], polymerization reactions [6], water sorption for heat transformation [7], pollutant sequestration [8], various synthesis manners and other attractive potential applications have attracted a huge deal of attention. Moreover, recently, extensive efforts of assessments resulted in several studies in the field of coordination compounds and novel group of material chemistry [9].

Chemistry of lead (II) coordination frameworks has attracted a great deal of attention, as a result of variable coordination number, its large ion radius, the likelihood of novel network topologies, a stereo-chemically active lone pair of $6s^2$ outer electrons, and interesting features [10]. Lead (II) includes an electronic structure of $[Xe]4f^{14}5d^{10}6s^2$. The 6s orbital stabilizes and contracts owing to the strong relativistic impacts in Au (I) occurring in close 6p metals, such as lead. The stabilized 6s pair participates less in the element's chemistry by being an "inert pair". This is the reason for the formation of compounds by inorganic lead within a lower oxidation state (less than the oxidation number 2) compared to what

its group number indicates. This may also influence the lead (II)-organic coordination compounds' stereochemistry [11].

The effect can be comprehended based on valence shell electron-pair repulsion or simple hybridization. Regarding its stabilization, it appears that the 6s orbital gives a "stereo-chemically active" 6s electron pair (or stereo-chemically active lone electron pair (SALEP)) by hybridizing with the 6p orbits. This fills a position in the metal's coordination sphere. Since the pair is not directly detectable, its existence is normally identified by a void within the coordination bonds distribution (hemidirected coordination, Scheme 1) [12]. Lack of the hybridization, only the s character is exhibited by the pair making it "stereo-chemically inactive." Therefore, a void or gap is not represented by the complex within the bond distribution (holodirected coordination; Scheme 1) [13].

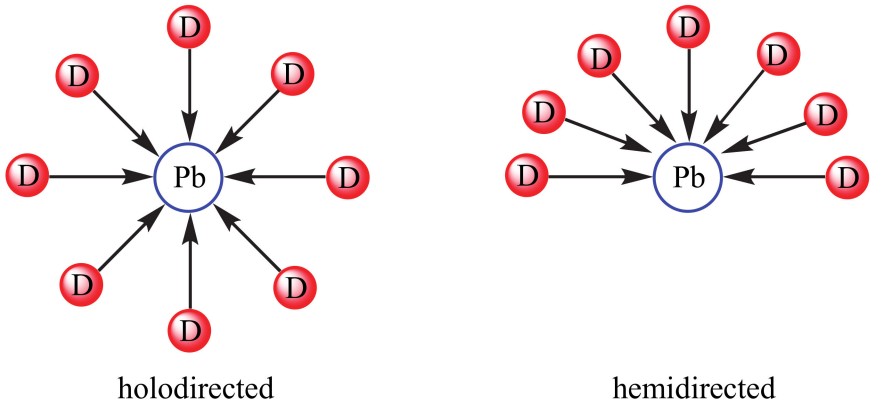

Scheme 1. *Holodirected* and *Hemidirected* arrangements of lead (II) coordination sphere (a ligand's D donor atom).

An ultrasound method leads to high-energy chemistry with processing acoustic cavitation, including bubbles, expansion, and their implosive collapse within a liquid intermediate [14]. In the ultrasound method, compressive and expansive acoustic waves are used to make and oscillate bubbles by irradiating liquids. Bubbles can invade and consequently collapse fast, i.e., with cooling and heating rates over 10^{10} Ks^{-1}. The huge energy concentration obtained over the collapse leads to a pressure of about one thousand bars and a local temperature of approximately 5000 K. The energy distribution to the surroundings during collapse and after the bounce causes the hot spot gas temperature to swiftly reach the temperature of the surrounding area. Ultrasonic irradiation can therefore be used to assist various chemical reactions progress at room temperature, and even certain reactions formerly difficult to actualize using conventional approaches [15,16].

Our team concentrated on the synthesis and design of metal organic coordination compounds. Recently, we provided reports on the preparation of various nano-metal organic coordination compounds [17–19]. Our next step in this regard is to assess the coordination behavior of lead (II) by pyridine-4-carbaldehyde thiosemicarbazone ligand. The organic ligand's structural chemistry is particularly fascinating owing to its multifunctional coordination manner (Scheme 2). A modest sonochemical synthesis route is described for this metal organic coordination system's nano-structure. Some new synthesis of nano lead(II) coordination polymer are reported in the literature [20–23].

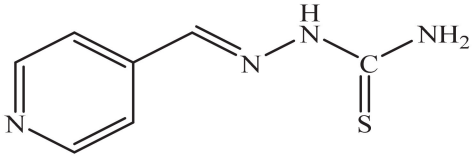

Scheme 2. Schematic of pyridine-4-carbaldehyde thiosemicarbazone ligand.

2. Experimental:

2.1. Instruments and Materials

All chemical compounds were bought from the Merck and Aldrich chemical companies. The pyridine-4-carbaldehyde thiosemicarbazone ligand (L) was prepared as a method described in the supporting information. A Bruker Vector 22 FT-IR (Richmond Scientific, Chorley, UK) spectrometer with KBr disks in the area of 400–4000 cm^{-1} was used for acquiring IR spectroscopy. An Electrothermal 9000 (Keison Products, Chelmsford, UK) apparatus determined the melting points. A multi-wave ultrasonic generator was utilized (Sonicator_3000; Misonix, Inc., Farmingdale, NY, USA). X'Pert diffractometer (produced with Panalytical, Panalytical, Malvern, UK) monochromatized CuK_{α} radiation was employed for performing measurements of PXRD. Mercury 2.4 was used for preparing simulated PXRD powder patterns in terms of the single-crystal data [24]. Elemental analyses were conducted utilizing a linked ISIS-300, Oxford EDS (Oxford Instruments, Abingdon, UK) (energy dispersion spectroscopy) detector. Chemical states and chemical compositions of the PbO nanoparticles were carried out through X-ray photoelectron spectroscopy (XPS) (Model: K-ALPHA, Thermo Fisher, Waltham, MA, USA).

The Scherrer formula was employed for estimating the crystallite size of chosen samples. Followed by gold coating Au, sample morphology was assessed using an SEM (Hitachi, Japan). Using an Xcalibur^{TM} diffractometer with a Sapphire2 CCD detector and Mo K_{α} radiation (monochromator Enhance, Oxford Diffraction Ltd., Abingdon, UK), and ω-scan rotation methods at 150 K, diffraction data were collected for the single crystal. The CrysAlis program package (Oxford Diffraction Ltd., UK) was utilized for data reduction and gathering, and refinement of cell parameters [25].

Multi-scan absorption modification with the CrysAlis (Rigaku, Tokyo, Japan) was utilized for the $[Pb(L)_2(CH_3COO)]_n$ data. By a full matrix weighted least-squares manner (SHELX-2014) (Free Software Foundation, Boston, MA, US) with the $w = 1/[\sigma^2(F_o)^2 + (0.035P)^2]$weight, where $P = (F_o^2 + 2F_c^2)/3$, we solved the structure by direct processes by SHELXS and adjusted on all F^2 data anisotropically. Mercury 2.4 was applied for creating molecular exhibits. Crystal data and arrangement modification are presented in Table 1, and the designated bond angles and lengths can be observed in Table 2 (for details, see Scheme S1, Supplementary Materials).

Table 1. The crystal data and structure refinements of complex.

Empirical formula	C_{16} H_{18} N_8 O_2 Pb S_2
Formula weight	625.69
Temperature	150(2) K
Wavelength	1.54178 Å
Crystal system	Monoclinic
Space group	Cc
Unit cell dimensions	a = 3.9618(1) Å α = 90° b = 43.0647(12) Å β = 91.669(2)° c = 12.0454(4) Å γ = 90°
Volume	2054.24(10) Å 3
Z	4
Density (calculated)	2.023 Mg/m3
Absorption coefficient	18.144 mm−1
F(000)	1200
Crystal size	0.100 × 0.005 × 0.004 mm3
Theta range for data collection	2.052 to 67.793°
Index ranges	−4 <= h <= 4, −50 <= k <= 50, −14 <= l <= 14
Reflections collected	12955
Independent reflections	3250 [R(int) = 0.0413]
Completeness to theta = 67.679°	99.5%
Absorption correction	Semi-empirical from equivalents
Maximum and minimum transmission	0.7530 and 0.4863
Refinement method	Full-matrix least-squares on F2

Table 1. *Cont.*

Data/restraints/parameters	3250/2/263
Goodness-of-fit on F2	1.020
Final R indices [I>2sigma(I)]	R1 = 0.0212, wR2 = 0.0466
R indices (all data)	R1 = 0.0225, wR2 = 0.0470
Absolute structure parameter	0.016(7)
Extinction coefficient	n/a
Largest diff. peak and hole	0.610 and −1.001 e. Å −3

Table 2. Chosen bond lengths [Å] & angles [°] for 1.

	Experimental	Calculated		Experimental	Calculated
Pb(1)-N(2)	2.573(6)	2.55	N(3)-C(2)	1.273(10)	1.30
Pb(1)-O(1)	2.605(6)	2.61	N(4)-C(6)	1.323(12)	1.35
Pb(1)-O(2)	2.638(5)	2.64	N(4)-C(5)	1.347(12)	1.35
Pb(1)-S(1)	2.7537(18)	2.86	N(5)-C(8)	1.316(10)	1.31
Pb(1)-S(1)#1	3.0770(18)	3.10	N(6)-N(7)	1.353(9)	1.36
Pb(1)-S(2)	3.1195(19)	3.12	N(6)-C(8)	1.362(10)	1.37
S(1)-C(1)	1.746(8)	1.74	N(6)-H(6)	0.8800	0.90
S(2)-C(8)	1.694(8)	1.70	N(7)-C(9)	1.271(11)	1.28
N(2)-Pb(1)-O(1)	124.1(2)	124	N(4)-C(5)-C(4)	123.5(9)	123
N(2)-Pb(1)-O(2)	131.15(18)	132	N(4)-C(5)-H(5C)	118.2	118
O(1)-Pb(1)-O(2)	49.47(16)	52	C(4)-C(5)-H(5C)	118.2	119
N(2)-Pb(1)-S(1)	58.17(14)	59	N(4)-C(6)-C(7)	124.2(8)	125
O(1)-Pb(1)-S(1)	85.40(13)	84	N(4)-C(6)-H(6A)	117.9	117
O(2)-Pb(1)-S(1)	73.15(13)	74	N(5)-C(8)-N(6)	117.1(7)	117
N(2)-Pb(1)-S(1)#1	84.03(15)	84	N(5)-C(8)-S(2)	124.5(6)	125
O(1)-Pb(1)-S(1)#1	137.89(12)	138	N(6)-C(8)-S(2)	118.3(6)	117
O(2)-Pb(1)-S(1)#1	88.60(13)	89	N(7)-C(9)-C(10)	120.3(7)	121
S(1)-Pb(1)-S(1)#1	85.41(5)	85	N(7)-C(9)-H(9A)	119.8	119
N(2)-Pb(1)-S(2)	70.38(14)	70	N(8)-C(12)-C(11)	123.0(7)	124
O(1)-Pb(1)-S(2)	77.92(12)	78	N(8)-C(12)-H(12A)	118.5	119
O(2)-Pb(1)-S(2)	127.08(13)	128	N(8)-C(13)-C(14)	123.9(8)	123
S(1)-Pb(1)-S(2)	100.85(5)	101	N(8)-C(13)-H(13A)	118.1	118
S(1)#1-Pb(1)-S(2)	144.19(5)	145	C(8)-S(2)-Pb(1)	114.3(3)	114
C(1)-S(1)-Pb(1)	84.6(3)	85	C(15)-O(1)-Pb(1)	95.3(5)	96
C(1)-S(1)-Pb(1)#2	100.7(3)	100	C(15)-O(2)-Pb(1)	94.4(4)	95
Pb(1)-S(1)-Pb(1)#2	85.42(5)	86	C(1)-N(2)-Pb(1)	101.2(5)	101

2.2. Synthesis of Nano-Structure of $[Pb(L)_2(CH_3COO)]_n$

The nano-structure of $[Pb(L)_2(CH_3COO)]_n$ was prepared using 10 mL of a 0.1 M solution of lead(II) acetate in water, and was placed in a high-density ultrasonic probe, and 10 mL of a solution containing 0.1 M of organic ligand in MeOH/H_2O was dropwise added. The achieved precipitates were filtered, rinsed by H_2O, and dried in air.

FT-IR(KBr) = (520, 1066, 1109, 1176, 1414, 1451, 1539, 1596, 3155, 3264, 3422) cm^{-1}.

2.3. Synthesis of Isolate Single Crystal of $[Pb(L)_2(CH_3COO)]_n$

Single crystals of $[Pb(L)_2(CH_3COO)]_n$ were isolated by putting lead(II) acetate (2 mmol) and organic ligand (2 mmol) in the key arm of a branched tube. MeOH was added cautiously to fill both arms. Sealing the tube, the ligand-comprising arm was submerged in an oil bath at 60 °C; however, the other arm was maintained at the ambient temperature. After 21 days, isolating and filtering off the crystals within the cooler arm, it was rinsed by ether and acetone, and air-dried.

FT-IR (KBr) = (650, 1016, 1050, 1128, 1438, 1473, 1541, 1612, 1652, 3131, 3249, 3428) cm^{-1}.

2.4. Synthesis of Lead (II) Oxide Clusters

A light yellow solution was formed after dissolving 0.2 mmol of $[Pb(L)_2(CH_3COO)]_n$ in 15 mL of oleic acid. The solution was degassed for 40 min and then heated to 180 °C for 1 h. Finally, a black precipitate was formed at the end of the reaction. A large excess of ethanol and a small amount of toluene were added to the solution; PbO clusters were separated by centrifugation. The final solids were washed with ethanol and dried in ambient air.

3. Results and Discussion

3.1. Investigation of L Ligand

In many carbazone ligands, enol-ketone tautomerization occurs. By tautomerization, hydrogen can bind to sulfur on a nitrogen atom adjacent to the thiocarbonyl ligand, and the ligand becomes negatively charged. As shown in Scheme 3, this tautomerization can also take place in the L ligand and, as a result, the bonding of the ligand to the enolate form is observed in the formation of the complex.

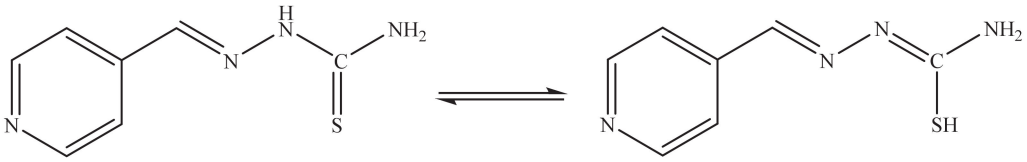

Scheme 3. Enol-ketone tautomerization of Schiff base L ligand.

The obtained ligands were identified using FT-IR spectroscopy. Figure 1 represents the FT-IR spectra of L ligand.

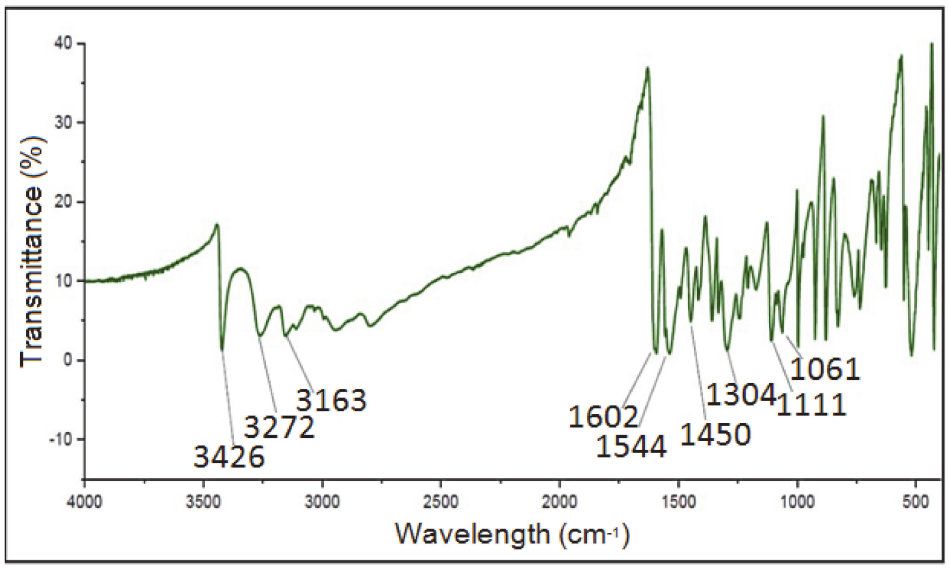

Figure 1. The FT-IR spectra of L ligand.

The results of FT-IR spectroscopy show that the band related to the amide tensile vibration for the L ligand in the region of 3426.47 cm^{-1} is observed as a sharp band. The most important band observed in the spectrum of Schiff base L ligands belongs to the imine functional group and the hydrogen on the nitrogen atom (—NH_2) of the ligands. Observing the band related to imine is proof of the formation of a Schiff Base product. The band corresponding to the imine $\nu_{C=N}$ for the L ligand is seen as a sharp band in the region of 1602.61 cm^{-1}.

Due to the structure of the synthetic ligand and the observation of a hydrogen atom attached to the nitrogen of the thiosemicarbazone, it is expected that this ligand will act

as a neutral ligand by retaining this hydrogen or act as an anionic ligand by losing this hydrogen. The related band $\nu_{N\text{-}H}$ for the L ligand is observed as a sharp band in the 3163.30 cm^{-1} region. The peak corresponding to $\nu_{C=S}$ for the L ligand is observed in the region of 1709 cm^{-1}. Due to the structure of the synthetic ligand, it is expected that this ligand will act as a mono-dentate or di-dentate ligand.

3.2. Investigation of $[Pb(L)_2(CH_3COO)]_n$

$[Pb(L)_2(CH_3COO)]_n$ was obtained as a novel one-dimensional fishbone coordination polymer from the reaction of lead(II) acetate by pyridine-4-carbaldehyde thiosemicarbazone (L).The nanostructure of the compound was determined in an aqueous solution through the ultrasound technique. The suitable single crystals of compound I for X-ray crystallography were obtained using the heat gradient of an aqueous solution based on the branched-tube method. Scheme 4 presents the two various routes utilized for preparing $[Pb(L)_2(CH_3COO)]_n$ materials.

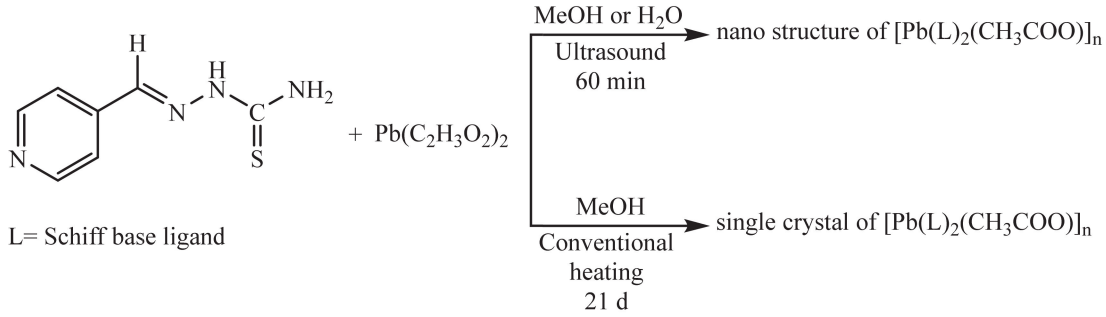

Scheme 4. Materials synthesized and synthetic manners.

Figure 2 displays the complex's FT-IR spectra in the bulk, crystalline, and nano shape. Comparison of these spectra demonstrates their similarity and the corresponding main peaks have a well overlap by each other.

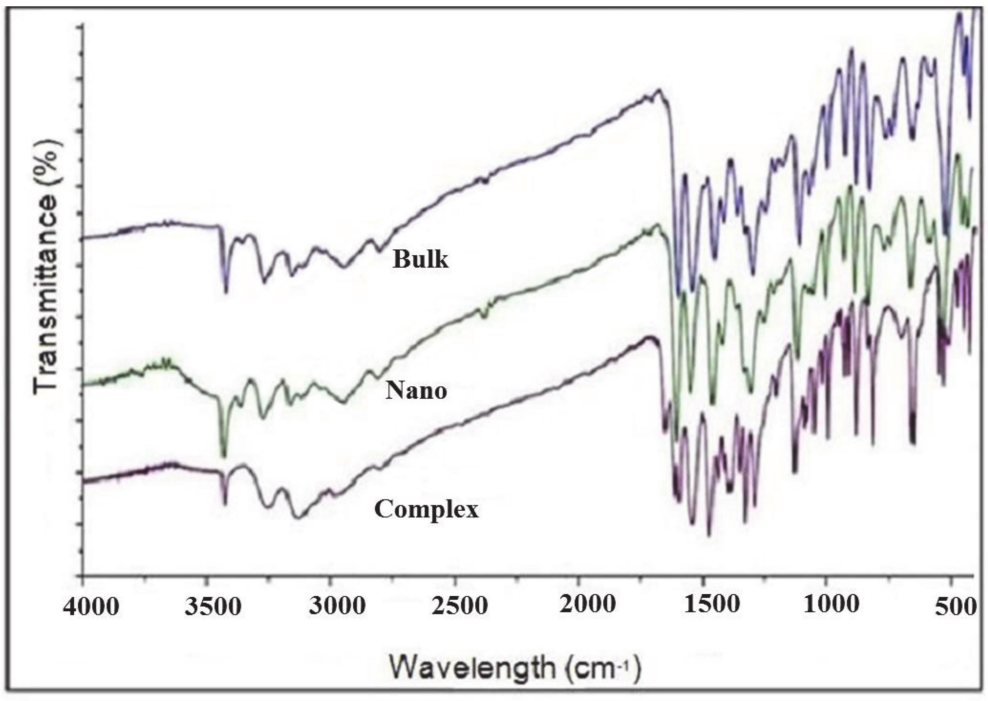

Figure 2. The FT-IR spectra of the $[Pb(L)_2(CH_3COO)]_n$ complex in the bulk, nano, and crystalline shape.

In the FT-IR spectrum of these compounds, absorption bands by varying intensities in the region of 1400–1600 cm^{-1} are attributed to the vibrations of the ligand pyridine ring, which is related to the C=N and C=C bonds. Peaks related to imine C=N are seen as sharp bands in the region of 1600 cm^{-1}, which have shifted to lower wavenumbers with the coordination of the ligand to the metal and the formation of a complex with little displacement.

The tensile N-H peaks in the vibrational spectrum of the complex are observed in the area of 3260 cm^{-1} and indicate the presence of the N-H group of the ligand when it is coordinated with the central metal, and indicate the presence of the ligand in the neutral form in the formation of the complex. For all three complexes, the related band of new C=N bond formation is not observed, and this proves that in the formation of all three complexes L ligand has participated in the form of ketones in the coordination of metallic ion. The C=S group in the complex is observed in the area of about 1730 cm^{-1} with a slight displacement, which indicates that it is coordinated to the metal.

The N-N group is observed in the 1050 cm^{-1} area that this adsorption band is shifted in the spectrum of all three complexes to lower wavenumbers than the spectrum of ligand, which indicates the lack of coordination of the nitrogen atom of azomethine to the metallic ion.

The results of these studies indicate that if ligand tautomerization takes place, the ligand participates in the formation of complexes in the form of enol, and in the spectrum of complexes the absorption band of $\nu_{N\text{-}N}$ is removed, and $\nu_{C\text{-}N}$ and $\nu_{N\text{-}N}$ shifts to higher numbers, and a new C = N bond is created in the wavenumber 1510–1560 cm^{-1}. However, the observation of $\nu_{N\text{-}N}$ band in the spectrum of complexes indicates that the ligand is not tautomerized in the solid-state and the presence of the ketonic form of the ligand in coordination with the metallic ion.

The $\nu_{C\text{-}H}$ aromatic bending is observed in the area of 880 cm^{-1}, and $\nu_{C\text{-}C}$ aromatic bending is observed in the area of 1450 cm^{-1}, and $\nu_{C\text{-}H}$ of the complex aromatic tensile in the area of 3150 cm^{-1} by a slight displacement, indicating that it is coordinated to the metal. As can be seen, there is a good match between the crystal, nanomaterial, and synthesized bulk in all areas.

The surface morphology of the synthesized nano coordination compound was investigated through the field emission scanning microscopy (FE-SEM) analysis. SEM assessments illustrate that obtained nanoparticles are of various sizes and have different shapes (Figure 3).

Figure 4 displays the simulated XPRD pattern of $[Pb(L)_2(CH_3COO)]_n$ in comparison to a nanostructure XRD pattern, Acceptable matches by slight differences in 2θ were found between the experimental and simulated XPRD patterns (Figure 4). It reveals that the synthesis obtained with the sonochemical manner as nanoparticles is equal to that obtained with crystallography. The considerable extending of the peaks denotes that the nanometer dimensions of the particles.

Determining the structure of coordination polymer $[Pb(L)_2(CH_3COO)]_n$, it was indicated that the complex crystallizes in the monoclinic system with space group Cc, taking the form of a two-dimensional polymer in the solid-state. The crystal structure of part of this complex's repeating unit is shown in Figure 5. In every single cell, we have four molecules, i.e., z = 4. The desired density is 2.023 Mg/m^3. The size of the crystal is 0.1 × 0.005 × 0.004 mm^3. a, b, c are different, but α and γ are 90°, and β is 91°.

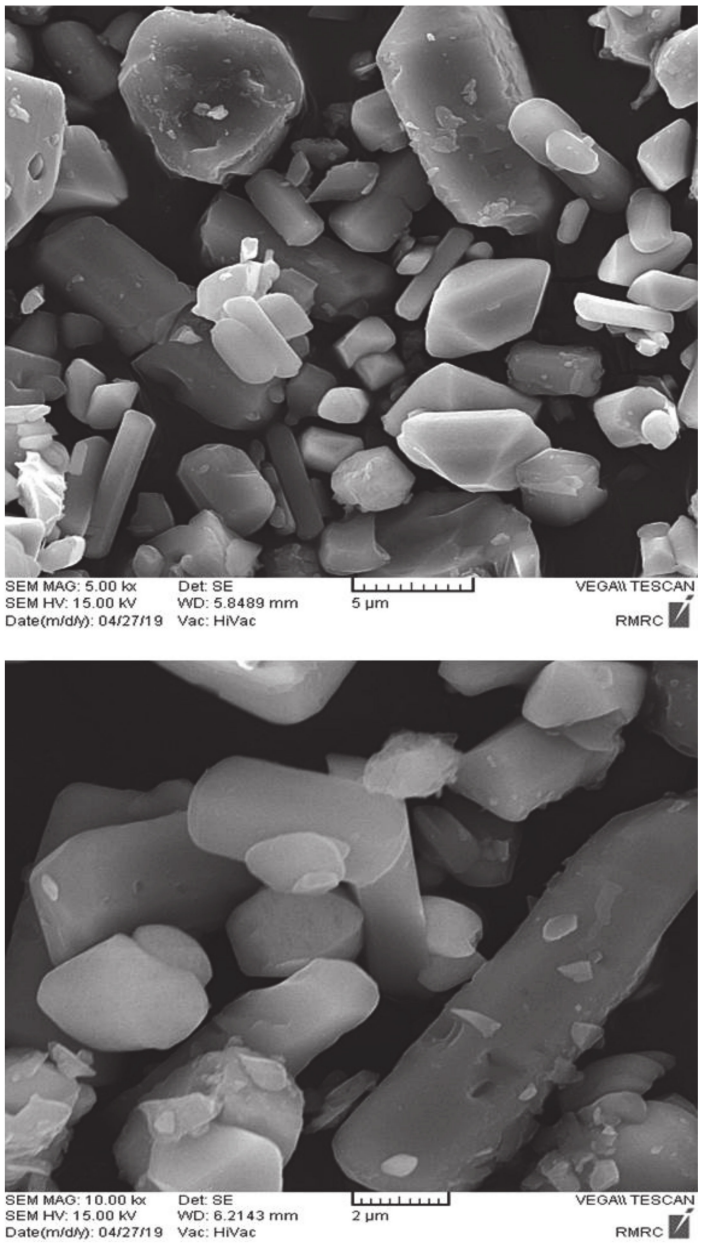

Figure 3. SEM images of the $[Pb(L)_2(CH_3COO)]_n$ at different magnifications.

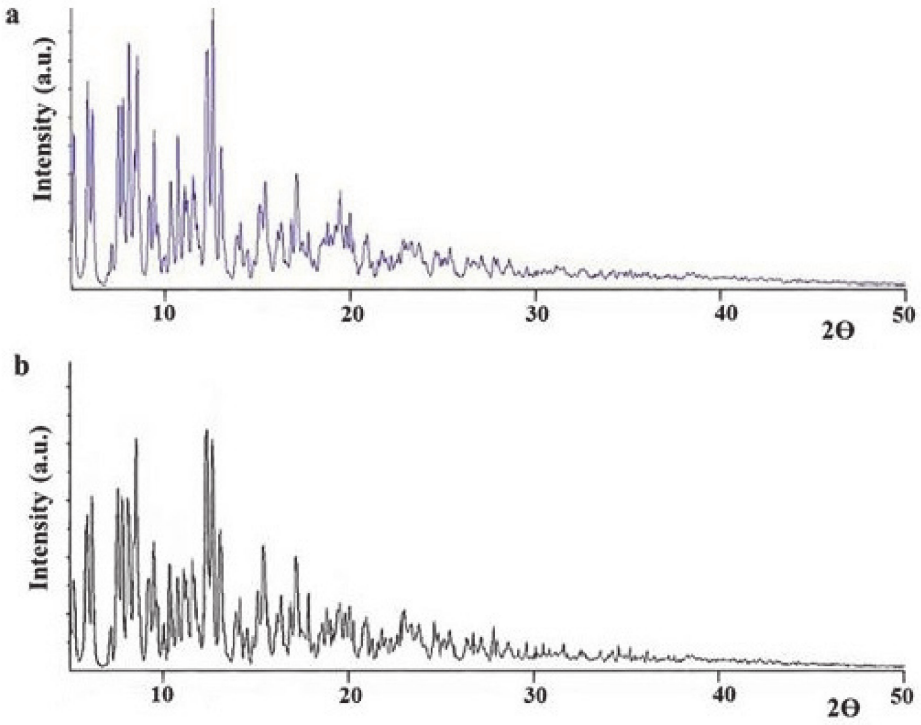

Figure 4. The XPRD designs of compound $[Pb(L)_2(CH_3COO)]_n$: **a** simulated from single crystal X-ray records and **b** nano structure of coordination polymer obtained within sonochemical technique.

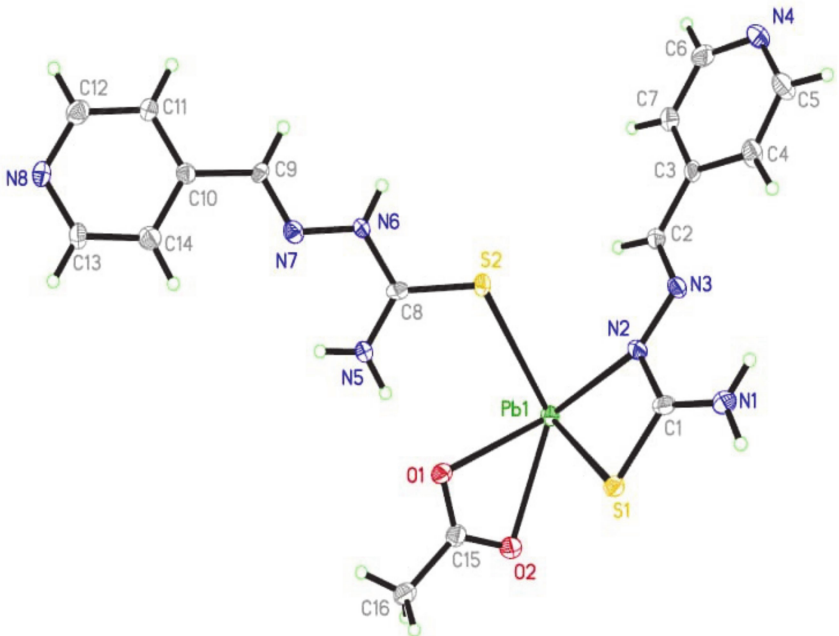

Figure 5. The crystal structure of $[Pb(L)_2(CH_3COO)]_n$.

In this type of combination, there is a type of lead with an asymmetric coordinated sphere. In the polymer chain structure, each lead metal center is attached to two oxygen atoms from the anionic acetate ligand, three sulfur atoms, and one nitrogen atom from the L-ligands. Therefore, lead has a coordination number of 6 with the $PbNS_3O_2$ schema. L-ligand acts as a two-dentate and single-toothed ligand in the polymer structure. This compound is in solid form as a one-dimensional coordination polymer. The compound's polymeric structure is shown in Figure 6.

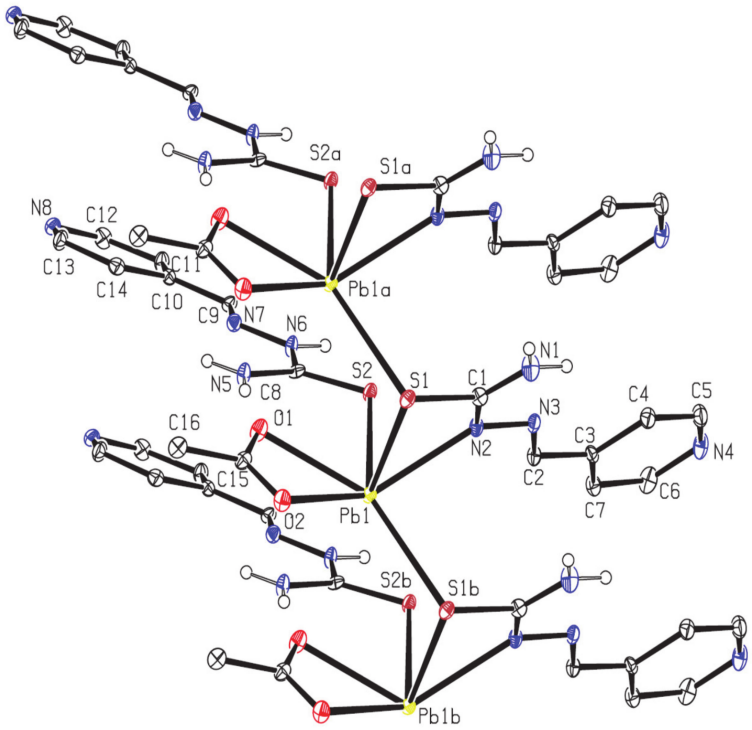

Figure 6. One-dimensional structure of coordination polymer.

In a coordination polymer, in addition to coordination covalent strong bonds, which cause the polymer to expand in a one-dimensional step, other weak interactions, such as hydrogen interactions and aromatic interactions cause the self-aggregation of one-dimensional chains and transform the structure into a three-dimensional super molecule with intermolecular interaction (Figure 7).

Figure 8 displays the thermal behavior of $[Pb(L)_2(CH_3COO)]_n$. The thermal gravimetric analysis (TGA) was performed within 25 °C–800 °C to study the single crystals' thermal stability. Followed by removing H_2O molecules from moisture at 80 °C to 102 °C, compound **1** was steady up to 174 °C. The decomposition with a mass loss of almost 64.75% occurred between 174 °C and 615 °C during three steps. The first step with a mass loss of 9.5% is attributed to removal of acetate molecule. The second and third part also corresponds to the exit of both ligand molecules with a mass loss of 29% in each step, respectively.

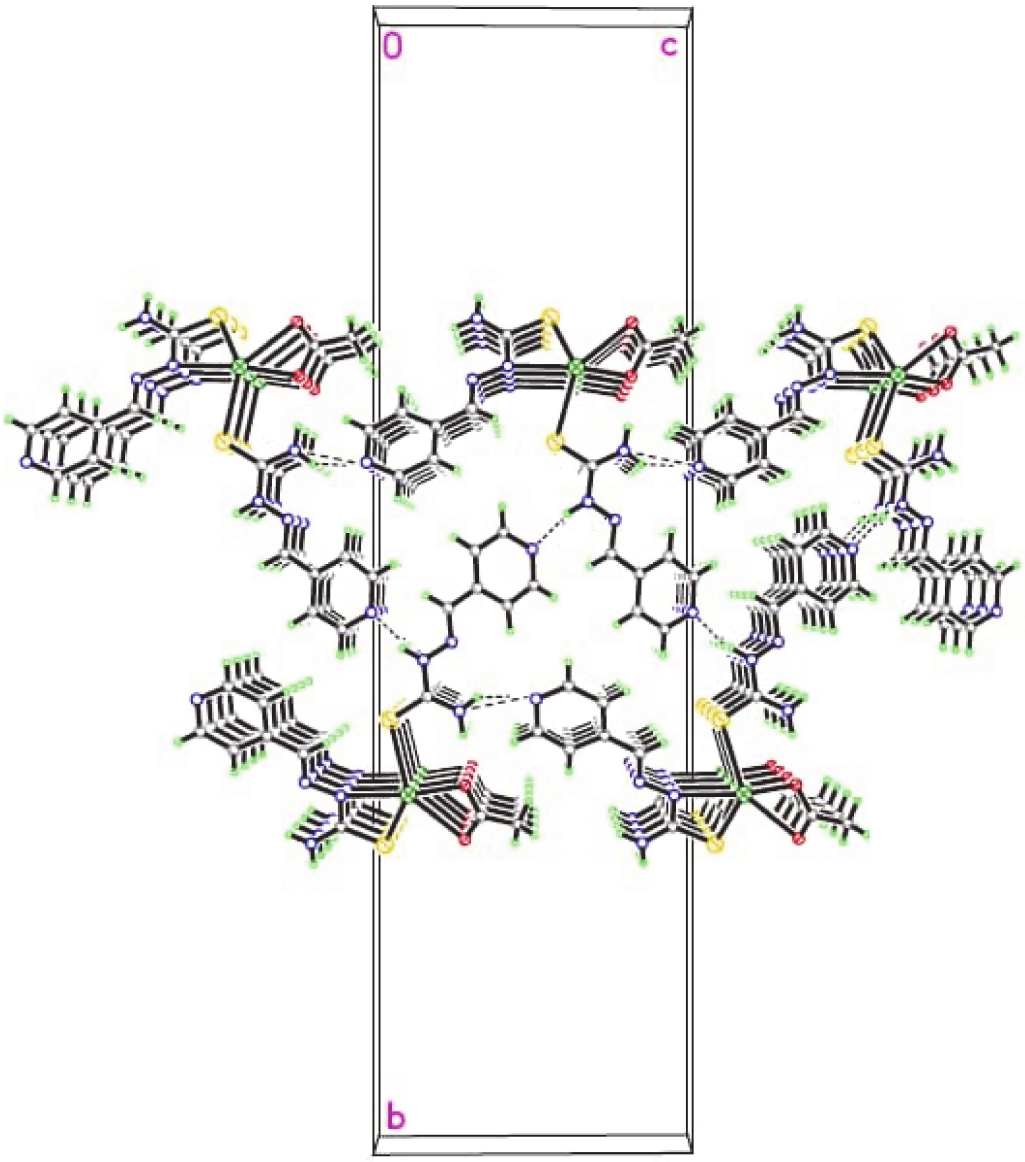

Figure 7. Packing the 1D chains to created 3D supramolecular layers via π–π interactions.

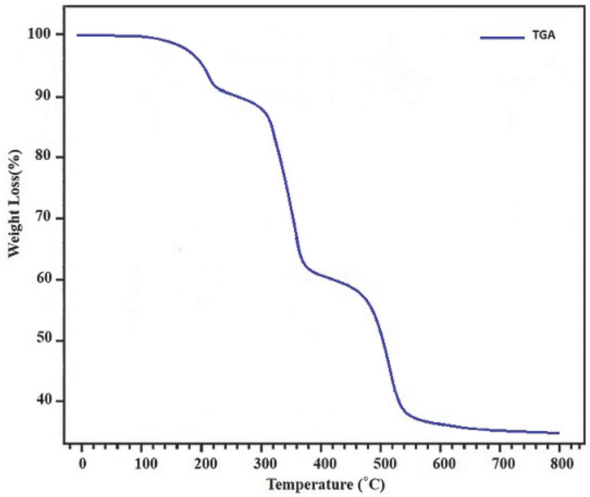

Figure 8. TGA curve of $[Pb(L)_2(CH_3COO)]_n$.

A solid residue created at around 800 °C was determined to be PbO based on the XPS results. Figure 9 displays the XPS spectra of PbO clusters. Two asymmetric peaks centered at 137.34 eV and 143.16 eV are attributed to the transitions of $4f_{7/2}$ and $4f_{5/2}$, respectively, and are assigned to Pb^{2+} ions in lead oxides lattice, which confirms that Pb^{2+} exists in the product in the form of PbO [26]. The O1 s spectrum for PbO indicates a peak at 531.2 eV closed to reported value in the literature, respectively [27].

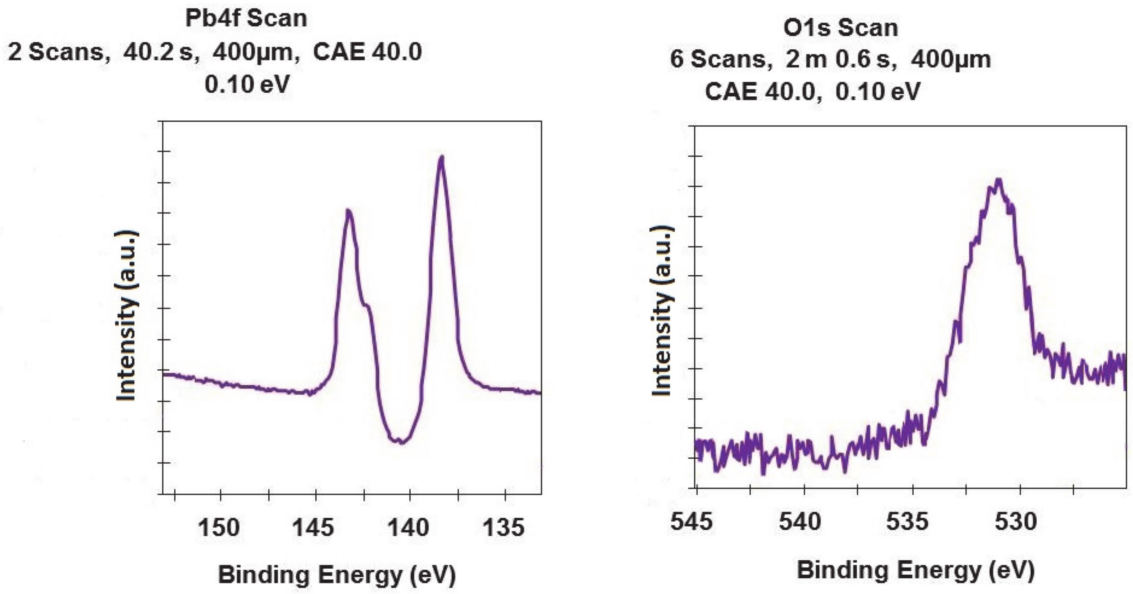

Figure 9. High-resolution XPS spectra of PbO clusters.

Moreover, the PbO clusters were obtained via thermolysis of $[Pb(L)_2(CH_3COO)]_n$ at 180 °C employing oleic acid as a surfactant. The XRD pattern of obtained lead oxide is shown in Figure 10, in which all the peaks are attributed to pure tetragonal phase of –α-PbO (JCPDS card file no. 85-0711).

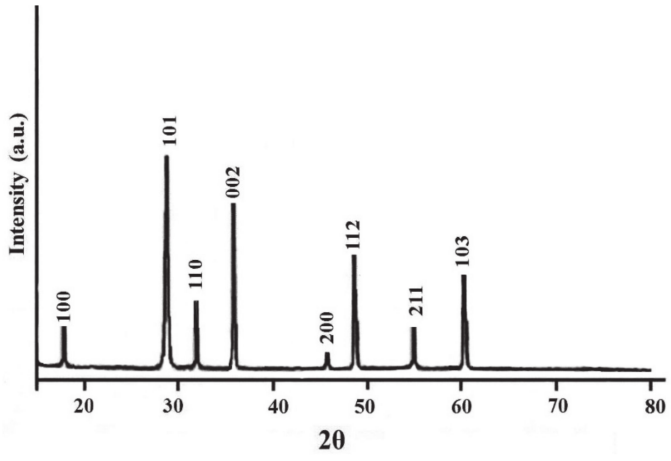

Figure 10. XRD pattern of Lead oxide clusters acquired by thermolysis of $[Pb(L)_2(CH_3COO)]_n$.

Moreover, the SEM image of PbO prepared by thermolysis represents a uniform shape of clusters with the average size of 15–65 nm, respectively (Figure 11).

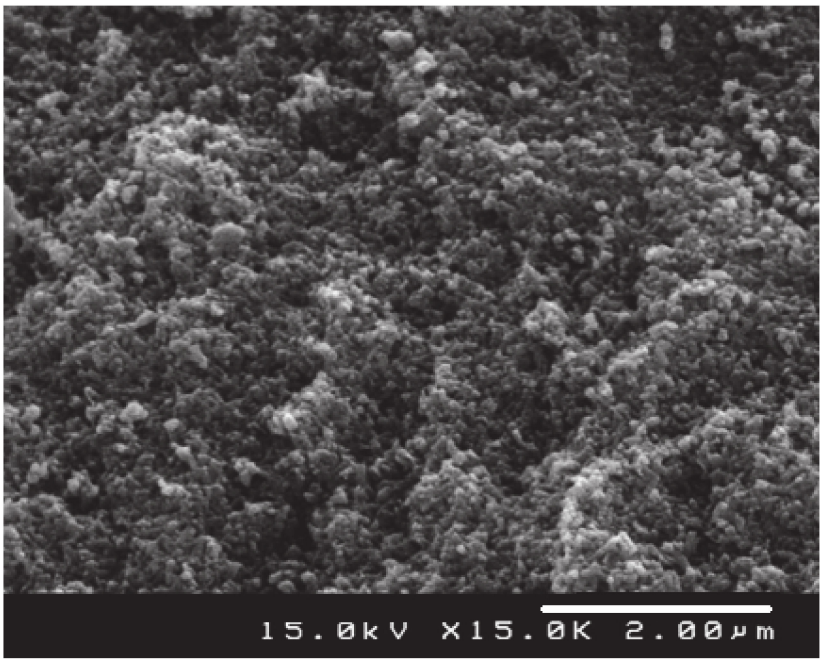

Figure 11. SEM image of the PbO clusters produced by the thermolysis of nanostructure of $[Pb(L)_2(CH_3COO)]_n$.

The TEM image of PbO clusters prepared by thermolysis is shown in Figure 12, which confirms the results obtained from SEM analyses.

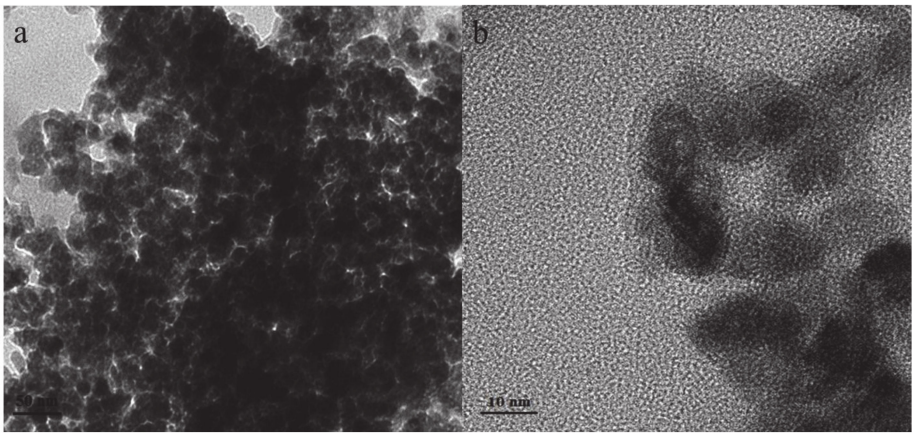

Figure 12. TEM image of the PbO clusters produced by the thermolysis of nanostructure of $[Pb(L)_2(CH_3COO)]_n$ at two magnifications (**a**) 50nm and (**b**) 10nm.

3.3. Computational Details

The geometry of the $[Pb(L)_2(CH_3COO)]_n$ complex were optimized using the B3LYP density functional model [28]. In these calculations, we used the 3–21G* basis set for C and H atoms, while the 6–31G* basis set was used for N and S atoms. For the Pb atoms, the LanL2DZ valence and effective core potential functions were used [29]. All DFT calculations were performed using the Gaussian 98 R-A.9 package [30]. X-ray structures were used as input geometries when available.

3.4. DFT Calculations

The calculated structural parameters are listed in Table 1. The significant figure is maintained to be four, which is sufficient for one bond length to be differentiated from the other. It should be noted that the experimental data belong to solid phase, whereas

the calculated data correspond to the isolated molecule in the gas-phase. However, the experimental and computational data in Table 2 clearly show that both data only slightly differ from each other. For example, the largest difference between experimental and calculated S1-Pb1 length is about 0.11 Å, while the biggest deviation occurs in the O1-Pb1-O2 angle by ca. 2.53°. As a result, the calculated geometrical parameters represent a good approximation.

The NBO charges of lead (II) and the coordinated atoms were also calculated. The positive charge of the lead (II) ions was 1.001. The considerably low positive charge in the lead (II) ion of **1** may be explained by its contribution to the Pb···Pb interactions. The charges of the S atoms of the ligands were −0.083, while the O atoms of acetate anions were −0.515 and −0.474. The charge of the N atoms of the ligands (in pyridine ring) was −0.035, while the charges of other N atoms of ligands were −0.077, −0.342, and −0.414.

The calculations indicate that complex **1** has 59 occupied molecular orbitals (MOs) for the $[Pb(L)_2(CH_3COO)]$ unit. The value of the energy separation between the highest occupied molecular orbital (HOMO) and the lowest unoccupied molecular orbital (LUMO) was calculated. Figure 13 shows the HOMO and LUMO for lead (II) complex. As seen in Figure 13, the HOMO and LUMO of the title complex are principally localized and delocalized among O atoms of one acetate anion. The calculated HOMO–LUMO gap is 0.1202 a.u. (3.275 eV). In compression by lead azide ($Pb(N_3)_2$) gap (4.7 eV)[31], this study found that the lead azide band gap is wider than the complex **1**. Therefore, it can be expected that the complex is primarily explosive and very sensitive to shock.

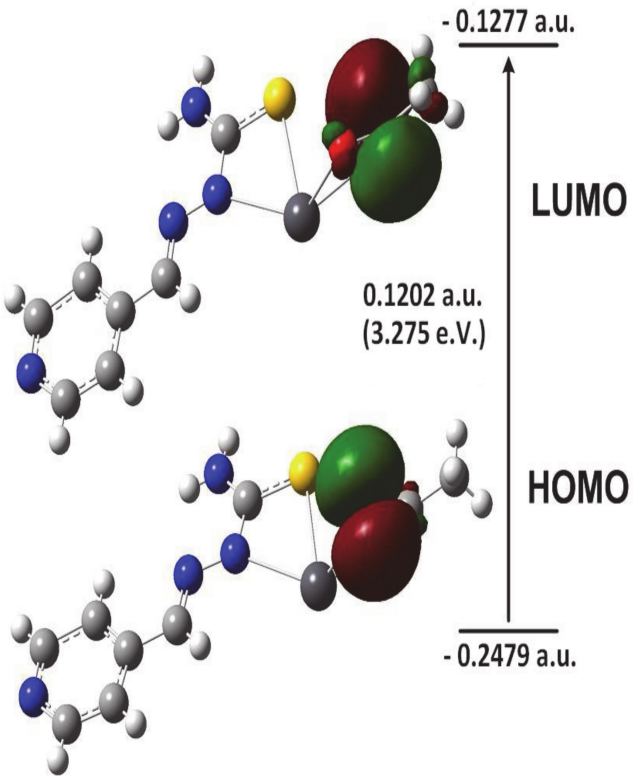

Figure 13. Frontier molecular orbitals for $[Pb(L)_2(CH_3COO)]$ unit.

4. Conclusions

In the present research, a new lead (II) coordination compound $[Pb(L)_2(CH_3COO)]_n$ nanostructure was synthesized in an ultrasound-assisted method and also compared with its crystal structure. The structural characterization of the new coordination polymer was carried out with SEM, single-crystal crystallography, elemental analysis, and IR spectroscopy. The complex's structure creates a stair-step 1D coordination polymer in solid-state. It was determined that the coordination number of Pb (II) ions is six by two

oxygen atoms from acetate anions and three sulfur atoms and one nitrogen atom from an organic ligand. By several weak interactions, the comprehensive system demonstrated a 3D structure. Thermolysis of new lead (II) coordination polymer results in uniform PbO nanoparticles. According to the computational DFT results, the HOMO and LUMO of the title complex are principally localized and delocalized among O atoms of one acetate anion. The estimated gap of HOMO–LUMO was 3.275 eV.

Supplementary Materials: The following are available online at https://www.mdpi.com/article/10.3390/cryst11060682/s1, Scheme S1. Cambridge Crystallographic Data Centre provided the crystallographic information for the structures as supplementary publication CCDC-2076593 for [Pb(L)2(CH3COO)]n (1). Duplicates of these data may be acquired by contacting de-posit@ccdc.cam.ac.uk by email or through official correspondence with CCDC, 12 Union Road, Cambridge CB2 1EZ, United Kingdom, Fax: +441223336033.

Author Contributions: J.D. writing—original draft preparation; Y.H., supervision, writing—review and editing; B.M., writing—review and editing; M.A. formal analysis; E.M.J. formal analysis; M.R., draft preparation and S.W.J., project administration and editing. All authors have read and agreed to the published version of the manuscript.

Funding: This work was funded by grant NRF-2019R1A5A8080290 of the National Research Foundation of Korea.

Institutional Review Board Statement: Not applicable.

Informed Consent Statement: Not applicable.

Data Availability Statement: Not applicable.

Acknowledgments: The authors thank Sayyed Jamaledin Asadabadi University and Qom University for their support.

Conflicts of Interest: The authors declare no conflict of interest.

References

1. Engel, E.R.; Scott, J.L. Advances in the green chemistry of coordination polymer materials. *Green Chem.* **2020**, *22*, 3693–3715. [CrossRef]
2. Lohe, M.R.; Gedrich, K.; Freudenberg, T.; Kockrick, E.; Dellmann, T.; Kaskel, S. Heating and separation using nanomagnet-functionalized metal–organic frameworks. *Chem. Commun.* **2011**, *47*, 3075. [CrossRef] [PubMed]
3. Li, J.R.; Sculley, J.; Zhou, H.C. Metal-organic frameworks for separations. *Chem. Rev.* **2012**, *112*, 869–932. [CrossRef] [PubMed]
4. Yi, F.Y.; Chen, D.; Wu, M.K.; Han, L.; Jiang, H.L. Chemical Sensors Based on Metal–Organic Frameworks. *ChemPlusChem* **2016**, *81*, 675–690. [CrossRef] [PubMed]
5. Zeng, L.; Guo, X.; He, C.; Duan, C. Metal–Organic Frameworks: Versatile Materials for Heterogeneous Photocatalysis. *ACS Catal.* **2016**, *6*, 7935–7947. [CrossRef]
6. Uemura, T.; Yanai, N.; Kitagawa, S. Polymerization reactions in porous coordination polymers. *Chem. Soc. Rev.* **2009**, *38*, 1228. [CrossRef]
7. Jeremias, F.; Khutia, A.; Henninger, S.K.; Janiak, C. MIL-100(Al, Fe) as water adsorbents for heat transformation purposes—a promising application. *J. Mater. Chem.* **2012**, *22*, 10148–10151. [CrossRef]
8. Doherty, C.M.; Knystautas, E.; Buso, D.; Villanova, L.; Konstas, K.; Hill, A.J.; Takahashi, M.; Falcaro, P. Magnetic framework composites for polycyclic aromatic hydrocarbon sequestration. *J. Mater. Chem.* **2012**, *22*, 11470. [CrossRef]
9. Liu, J.Q.; Luo, Z.D.; Pan, Y.; Singh, A.K.; Trivedi, M.; Kumar, A. Recent developments in luminescent coordination polymers: Designing strategies, sensing application and theoretical evidences. *Coord. Chem. Rev.* **2020**, *406*, 213145. [CrossRef]
10. Engelhardt, L.M.; Furphy, B.M.; Harrowfield, J.M.; Patrick, J.M.; White, A.H. 1:1 Adducts of lead(II) thiocyanate with 1,10-phenanthroline and 2,2′,6′,2"-terpyridine. *Inorg. Chem.* **1989**, *28*, 1410. [CrossRef]
11. Shimonni-Livny, L.; Glusker, J.P.; Bock, C.W. Lone Pair Functionality in Divalent Lead Compounds. *Inorg. Chem.* **1998**, *37*, 1853–1867. [CrossRef]
12. Imran, M.; Mix, A.; Neumann, B.; Stammler, H.G.; Monkowius, U.; Gründlinger, P.; Mitzel, N.W. Hemi- and holo-directed lead(ii) complexes in a soft ligand environment. *Dalt. Trans.* **2014**, *44*, 924–937. [CrossRef]
13. Zhu, X.; Li, Y.; Zhang, S.; Liu, R.; Qian, G.; Zhang, H.; Gao, J. Two new crystal structures of two-dimensional lead(II) coordination polymers with flexible alicyclic carboxylate ligands. *Inorg. Nano-Metal Chem.* **2017**, *47*, 717–721. [CrossRef]
14. Pokhrel, N.; Vabbina, P.K.; Pala, N. Sonochemistry: Science and Engineering. *Ultrason Sonochem.* **2016**, *29*, 104–128. [CrossRef]
15. Mason, T.J. Ultrasound in synthetic organic chemistry. *Chem. Soc. Rev.* **1997**, *26*, 443–451. [CrossRef]
16. Suslick, K.S.; Price, G.J. Applications of ultrasound to materials chemistry. *Ann. Rev. Mater. Sci.* **1999**, *29*, 295–326. [CrossRef]

17. Hanifehpour, Y.; Dadashi, J.; Mirtamizdoust, B. Ultrasound-Assisted Synthesis and Crystal Structure of Novel 2D Cd (II) Metal–Organic Coordination Polymer with Nitrite End Stop Ligand as a Precursor for Preparation of CdO Nanoparticles. *Crystals* **2021**, *11*, 197. [CrossRef]
18. Mirtamizdoust, B.; Hanifehpour, Y.; Behzadfar, E.; Roodsari, M.S.; Jung, J.H.; Joo, S.W. A novel nano-structured three-dimensional supramolecular metal-organic framework for cadmium (II): A new precursor for producing nano cadmium oxide. *J. Mol. Struct.* **2020**, *1201*, 127191. [CrossRef]
19. Mirtamizdoust, B. Sonochemical synthesis of nano lead(II) metal-organic coordination polymer; New precursor for the preparation of nano-materials. *Ultrason Sonochem.* **2017**, *35*, 263–269. [CrossRef]
20. Akhbari, K.; Morsali, A.; Retailleau, P. Effect of two sonochemical procedures on achieving to different morphologies of lead (II) coordination polymer nano-structures. *Ultrason. Sonochemistry* **2013**, *20*, 1428–1435. [CrossRef]
21. Sadeghzadeh, H.; Morsali, A. Hedge balls nano-structure of a mixed-ligand lead (II) coordination polymer; thermal, structural and X-ray powder diffraction studies. *CrystEngComm* **2010**, *12*, 370–372. [CrossRef]
22. Ranjbar, Z.R.; Morsali, A. Sonochemical syntheses of a new nano-sized porous lead (II) coordination polymer as precursor for preparation of lead (II) oxide nanoparticles. *J. Mol. Struct.* **2009**, *936*, 206–212. [CrossRef]
23. Li, B.; Huang, D.; Zhang, T.; Niu, X.; Liu, J.; Zhang, W.; Liu, Y.; Liu, Z.; Zhang, P.; Li, J. Five lead (II) coordinated polymers assembled from asymmetric azoles carboxylate ligands: Synthesis, structures and fluorescence properties. *Inorg. Chim. Acta* **2021**, *514*, 120035. [CrossRef]
24. Mercury 2.4, Copyright Cambridge Crystallographic Data Centre: 12 Union Road; Cambridge, UK.
25. Oxford Diffraction. *CrysAlis RED and CrysAlis CCD Software (Ver. 1.171.32.5)*; Oxford Diffraction Ltd.: Abingdon, UK, 2010.
26. Gautier, C.; Muller, M.C.; Averous, M. Study of PbSe layer oxidation and oxide dissolution. *Appl. Surf. Sci.* **1999**, *141*, 157–163. [CrossRef]
27. Zingg, D.S.; Hercules, D.M. Electron spectroscopy for chemical analysis studies of lead sulfide oxidation. *J. Phys. Chem.* **1978**, *82*, 1992. [CrossRef]
28. Becke, A.D. Density-functional thermochemistry.III. The role of exact exchange. *J. Chem. Phys.* **1993**, *98*, 5648. [CrossRef]
29. Hay, P.J.; Wadt, W.R. Ab initio effective core potentials for molecular calculations. Potentials for the transition metal atoms Sc to Hg. *J. Chem. Phys.* **1985**, *82*, 270. [CrossRef]
30. Frish, M.J.; Trucks, G.W.; Schlegel, H.B.; Scuseria, G.E.; Robb, M.A.; Cheeseman, J.R.; Zakrzewski, V.G.; Montgomery, J.A., Jr.; Stratmann, R.E.; Burant, J.C.; et al. *GAUSSIAN 98, Revision A.9*; Gaussian Inc.: Pittsburgh, PA, USA, 1998.
31. Younk, E.H.; Kunz, A.B. An ab initio investigation of the electronic structure of lithium azide (LiN_3), sodium azide (NaN_3), and lead azide [$Pb(N_3)_2$]. *Int. J. Quantum Chem.* **1997**, *63*, 615–621. [CrossRef]